Functional Magnetic Resonance Imaging in Medicine and Physiology

CHRIT T. W. MOONEN, PETER C. M. VAN ZIJL, JOSEPH A. FRANK, DENIS LE BIHAN, EDWIN D. BECKER

Magnetic resonance imaging (MRI) is a well-established diagnostic tool that provides detailed information about macroscopic structure and anatomy. Recent advances in MRI allow the noninvasive spatial evaluation of various biophysical and biochemical processes in living systems. Specifically, the motion of water can be measured in processes such as vascular flow, capillary flow, diffusion, and exchange. In addition, the concentrations of various metabolites can be determined for the assessment of regional regulation of metabolism. Examples are given that demonstrate the use of functional MRI for clinical and research purposes. This development adds a new dimension to the application of magnetic resonance to medicine and physiology.

NUCLEAR MAGNETIC RESONANCE (NMR) IS BASED ON THE absorption of radio-frequency (RF) energy by the magnetic moments of atomic nuclei in samples placed in a strong magnetic field. The sensitivity of NMR parameters to local chemical environment and to molecular mobilities has long allowed NMR to be used for structural studies and compound identification. In 1973, Lauterbur added an entirely new aspect to the already vast array of emerging NMR methodologies, namely image formation based on NMR principles (*1*). This achievement has led to the highly successful application of NMR imaging (or "MRI") to clinical medicine.

Conventional MRI of the human body relies mainly on the detection of the most abundant type of nuclei, the hydrogens in water (and to some extent, fat). For discrimination of healthy and diseased tissues, adequate contrast is essential. Such contrast depends not only on differences in water concentration, but also on the NMR relaxation times T_1 and T_2 (see below), which in turn are related to local mobilities and interactions (*2*). However, our understanding of tissue water relaxation is still incomplete as a consequence of the very complex intracellular environment (*3*). Thus, in the clinical setting, an empirical knowledge of differences in relaxation parameters is used to obtain optimal contrast between normal and pathological tissue, but the information is limited to macroscopic structure and anatomy (*4*).

Recent developments in MRI have demonstrated the possibility of adding function parameters to the information content. Sequential images of kinematic changes in macroscopic anatomical features (*5, 6*), such as those that occur during joint motion or cardiac contraction, are examples of functional MRI. Several rapid imaging methods have been proposed (*7, 8*) that can be used to visualize such processes. Since their purpose is to study macroscopic (dynamic) anatomy, we shall not include them in this review. Rather, we concentrate on two new branches of functional imaging that measure function on the microscopic or molecular level, namely (i) imaging of molecular displacements and (ii) metabolite (or spectroscopic) imaging. The first group of methods relates to various forms of transport. Diffusion, flow, and exchange are crucial elements for the complex processes in living systems. The second group provides information about the regulation of metabolism. We present the principles of these techniques, each accompanied by a practical example, and compare them with more established functional imaging techniques such as positron emission tomography (PET), single-photon emission computed tomography (SPECT), and conventional radiological techniques.

Magnetic Resonance Properties for Studying Function

Before describing the specific methods for functional MRI, we review briefly some of the basic properties of nuclear magnetic moments in a magnetic field (Fig. 1). The combined nuclear moments give rise to a total magnetization along the axis of the external magnetic field B_0 (Fig. 1A). By convention this axis is labeled z and the magnetization along it is called longitudinal. Upon perturbation by a short RF pulse, this magnetization is brought into the xy or transverse plane, where it precesses with the Larmor frequency

$$\omega = \gamma B_{\text{nucleus}} \quad (1)$$

where γ is a nuclear constant. The magnetic field at the nucleus (B_{nucleus}) results primarily from the field B_0 imposed on the sample but is modified by the chemical environment through chemical bonds and through space. Thus nuclei in different environments have slightly different resonance frequencies as expressed in their values of nuclear shielding or chemical shift. With the inclusion of

The authors are at the National Institutes of Health, Bethesda, MD 20892. C. T. W. Moonen is at the In Vivo NMR Research Center, Building 10, Room B1D-123 National Center for Research Resources. P. C. M. van Zijl is a guest researcher at the National Cancer Institute from Georgetown University Medical School, Department of Pharmacology, Washington, DC 20007. J. A. Frank is with the Diagnostic Radiology Department of the Clinical Center and at the Department of Radiology and Internal Medicine, Georgetown University Medical School. D. Le Bihan is with the Diagnostic Radiology Department of the Clinical Center. E. D. Becker is with the Laboratory of Chemical Physics, National Institute of Diabetes and Digestive and Kidney Diseases.

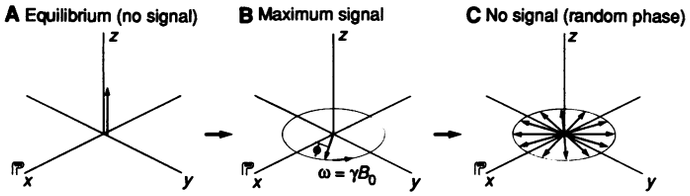

Fig. 1. (**A**) Equilibrium situation for an ensemble of nuclei in a magnetic field oriented along the z-axis. The net nuclear magnetization aligns along z, parallel to the external field, as shown by the arrow. No signal is detected by the receiver (shown along the x-axis) because magnetization and the receiver are perpendicular. (**B**) After a perturbation with a radio-frequency (RF) field, the magnetization is in the xy, or transverse, plane and precesses around the z-axis. Its position in time is given by phase $\phi = \omega t$, with ω the Larmor precession frequency depending on the local field (Eqs. 1 to 3). (**C**) Situation of random distribution of phase in the transverse plane after all nuclei have experienced different magnetic fields. No signal is detected since positive and negative components compensate.

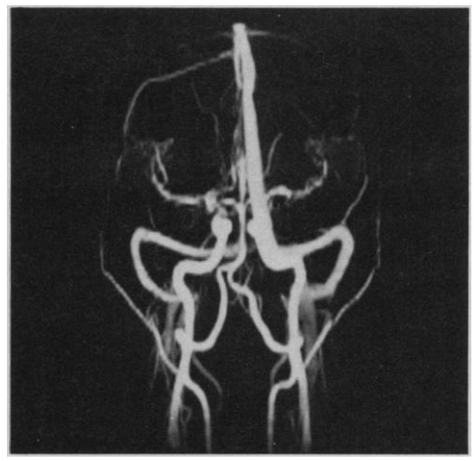

Fig. 2. Flow imaging of the human head. Detailed information of the major vessels is shown in an anterior-posterior projection. Acquisition details: Data obtained in a three-dimensional matrix (256 by 256 by 128 resolution elements) with a phase-contrast MRI method. Three data sets, each with sensitivity to flow along mutually orthogonal axes, were combined to produce the total-flow image. Field strength, 1.5 T. [Courtesy of C. L. Dumoulin and S. P. Souza, General Electric Corporate Research and Development Center, Schenectady, New York]

the shielding σ, the Larmor equation becomes

$$\omega = \gamma B_0(1 - \sigma) \quad (2)$$

For a single chemical species, such as the hydrogens in water, the precessing magnetization induces an electric signal, oscillating at frequency ω, in the RF coil aligned along the x-axis in Fig. 1. At time t, the position of the magnetization in the transverse plane describes an angle ϕ with the receiver axis (the phase), which is related to the resonance frequency ω by $\phi = \omega t$ (Fig. 1B). Immediately after application of the RF pulse, all spins have equal phase and a maximum signal is detected. Since the resonance frequency depends on the magnetic field that the nuclei experience, local field fluctuations (such as those caused by neighboring nuclei and electrons) may change this frequency. After a period of time, this range of frequencies leads to a spread in phase and no signal is detected, since for each positive component there is a compensating negative one (Fig. 1C). The time constant describing this phase dispersion is T_2, the transverse relaxation time. Concurrently, but over a longer period of time, the z-component of the magnetization returns to its equilibrium situation (Fig. 1A) with a time constant T_1, the longitudinal relaxation time. For example, in brain, water has a T_2 of the order of 100 ms while T_1 may be 1 to 2 s depending on the magnetic field strength used (*3*).

The innovative feature that permits NMR to be used for imaging is the application of a magnetic field gradient $G = dB_0/dr$ in the direction r. Since the gradient causes a different field ($B_0 + Gr$) at each location r in the sample along the direction of the gradient, the resonance frequencies of nuclei of the sample are labeled by their locations according to the modified Larmor equation

$$\omega = \gamma(B_0 + Gr)(1 - \sigma) \quad (3)$$

Several efficient methods for encoding the spatial information in two or three dimensions are in use (*2, 3, 9*), the most common of which use two-dimensional Fourier transform methods to label orthogonal directions according to phase and frequency (*10*). Such NMR images usually consist of 256 by 256 volume elements (voxels) in a field-of-view of about 120 to 400 mm for each axis in the plane and a plane thickness of 1 to 10 mm. Such a volume element provides adequate signal-to-noise ratio for detection of the hydrogen nuclei of water in the human body. Our discussion in this article is limited to NMR of water (in which σ in Eq. 3 is a constant) except for the later section on metabolite imaging.

In summary, the ensemble of nuclei is characterized by five parameters: (i) magnitude of the longitudinal magnetization; (ii) phase and magnitude of the transverse magnetization; (iii) resonance frequency; (iv) longitudinal relaxation time T_1; and (v) transverse relaxation time T_2. A change in one of these parameters may be caused by a function, such as blood flow, and may thus be used to visualize or quantify that particular function (see below). The intensity of volume elements in the resulting functional image is no longer determined by the usual parameters of concentration, T_1 and T_2 of water, but by the functional parameter, for example, the velocity of blood flow.

Flow Imaging

Imaging of flow has diagnostic value, because abnormal blood flow in vessels is related to many diseases, such as cerebral vascular disease and coronary heart disease. Long before MRI was developed, NMR methods were used for the measurement of flow (*11*). When MRI techniques were first being applied, flow effects were encountered as rather annoying image artifacts. However, in modern MR angiography (visualization of the vascular system), flow information is accurately depicted. It may be based on changes in either the magnitude of the longitudinal magnetization [often referred to as time-of-flight MR angiography (*12*)] or in the phase of the transverse magnetization [usually termed phase-contrast MR angiography (*13*)]. The time-of-flight approach relies on inflow into a detection plane by nuclei whose longitudinal magnetization has been perturbed (decreased) at another location, usually by a saturating RF field. It is a direct method, particularly useful for the study of large vessels, such as the carotid artery bifurcation. It is less prone to motion artifacts because the source of information is the longitudinal magnetization. However, its information content is limited to flow from the location where the perturbation was achieved to the imaged plane.

In phase-contrast methods flow encoding can be carried out by applying a bipolar gradient pulse, that is, two successive field gradient pulses of opposite sign (strength of the order of 0.01 T/m) but equal duration δ (of the order of 2 ms depending on actual velocity) without delay between them. During the period δ of the first gradient, the resonance frequency of a nucleus at location r is changed by an amount ω_r (Eq. 3) and, similar to Fig. 1B, the precessing magnetization acquires a phase increment $\phi = \omega_r\delta$. If the

nucleus remains at position r during the second half of the bipolar pulse, the phase change acquired during the first part is exactly canceled. However, if the position of the nucleus has changed between the two gradient pulses, because of flow, for example, the phase cancellation is incomplete. Since the resulting net phase shift is to first order proportional to the velocity, the latter quantity (in the direction of the field gradient) can be quantified based on the change in phase. This principle in its simplest form is referred to as a flow-dephasing method, and the gradients are called flow-encoding gradients. The signal of stationary nuclei is avoided by repeating the basic experiment with the bipolar gradient reversed in sign, thereby creating a sign-reversed phase due to flow and an equal phase for stationary nuclei. Thus vectorial subtraction of transverse magnetization leads to cancellation of all signal of stationary nuclei. This approach yields a high information density, because all flow in the direction of the phase-encoding gradients can be detected. The method has to be repeated with the flow-encoding gradient in different directions to describe the velocity in three-dimensional space.

Detailed information of the major vessels in the human head can be obtained by using phase-contrast MR angiography (Fig. 2). However, the method has some drawbacks. First, signal can be lost as a result of velocity and direction distributions within one volume element. The resulting phase dispersion (Fig. 1C) may lead to an underestimation of the regional flow velocity and thus hampers quantification. This problem may be alleviated by using a stepwise increase of the gradient strength of the flow-encoding gradients (*14*). Second, since the method detects displacements, special care must be taken to avoid macroscopic motion between the two experiments, for example, due to the cardiac or respiratory cycle.

Since blood flow in the human body is mostly pulsatile, MR angiographic methods have recently been designed to measure the time dependence of flow velocity (*15*). Another approach is to measure the acceleration of flow using specially designed gradient pulses (*16*).

Of the more established flow imaging techniques, ultrasound is the least expensive. However, deep and small vessels are difficult to analyze, especially in the vicinity of bone. An often used alternative approach is the tracing of a bolus of iodine contrast agent by succesive x-ray images. This method offers superior spatial resolution and a high information content, but is invasive because of the need of catheterization and the use of ionizing radiation. Also, adverse effects of iodine may pose safety concerns.

MR angiography techniques can also be applied to body fluids other than blood, for example, cerebrospinal fluid (CSF) (*17*). Often, the urgency of a neurosurgical procedure is dictated by the severity of alterations in CSF circulation and its relation to brain and spine function. However, conventional methods for evaluating CSF circulation require the injection of a tracer into the CSF spaces, for instance, through a lumbar or occipital puncture (*18*).

Diffusion Imaging

Whereas the previous method identifies coherent displacements of fluids, incoherent (random) displacements, like diffusion, may also be studied by measuring changes in transverse magnetization. Again, the history of this type of measurement goes back to the first years of NMR research (*19*), when the principles of in vitro molecular diffusion effects on magnetic properties were outlined. In vitro random displacements are a consequence of Brownian motion. In vivo, boundaries of compartments, active and passive transport processes, adsorption to macromolecules, and local differences in flow velocity and direction may all influence incoherent displacements (*20–22*). Since all incoherent motions inside a volume element (voxel) are measured, the name intravoxel incoherent motion (IVIM) imaging is a better description than "diffusion" imaging (*20, 21*). Diffusion can also be measured with the bipolar gradient pulse described above for flow measurement (*23*). Because of the diffusional displacement, rephasing during the second gradient pulse is incomplete. As a result of the random nature of molecular motion in diffusion, a phase dispersion is caused, thus leading to a decrease in the signal amplitude (*24*). The duration δ of the gradient pulses and the time Δ between their starts are usually longer for diffusion imaging than for flow imaging, since diffusional displacements are smaller. The residual signal amplitude S following a bipolar gradient is related to that in the absence of the gradient S_0 by

$$\ln(S/S_0) = -\gamma^2 G^2 \delta^2 (\Delta - \delta/3) D \quad (4)$$

where D is the diffusion coefficient. This concept has only recently been proposed for imaging (*20, 25*).

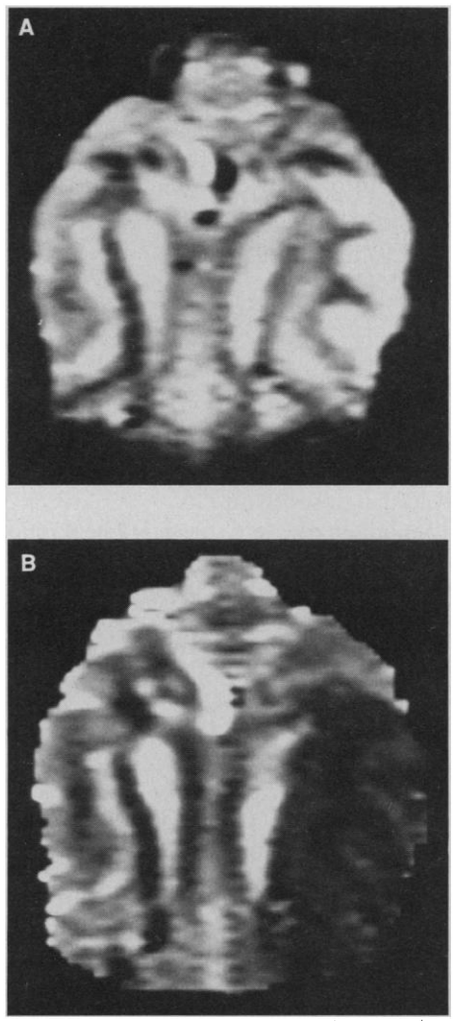

Fig. 3. Transverse images of cat brain following occlusion of the middle cerebral artery. (**A**) Conventional image: some hyperintensity is seen on the right side of the infarcted area, but the boundaries of the affected region are not clearly outlined. (**B**) Calculated diffusion image showing the diffusion coefficient for each voxel. The area with the lowered diffusion coefficient corresponds accurately with the ischemic region. The artery was occluded 6 hours before acquisition of these images. Acquisition details: stimulated echo image (displayed as 128 by 128 volume elements); echo time, 80 ms; repetition time, 5 s; diffusion time, 143 ms; diffusion gradients of 12.5-ms duration and 0.035 T/m in the horizontal direction of the image; slice thickness, 3 mm; total acquisition time, 5 min (cardiac gated); and field strength, 4.7 T. [Courtesy of C. T. W. Moonen, M. H. M. de Vleeschouwer, D. DesPres, J. Pekar, and P. C. M. van Zijl, In Vivo NMR Research Center, National Institutes of Health, Bethesda, Maryland]

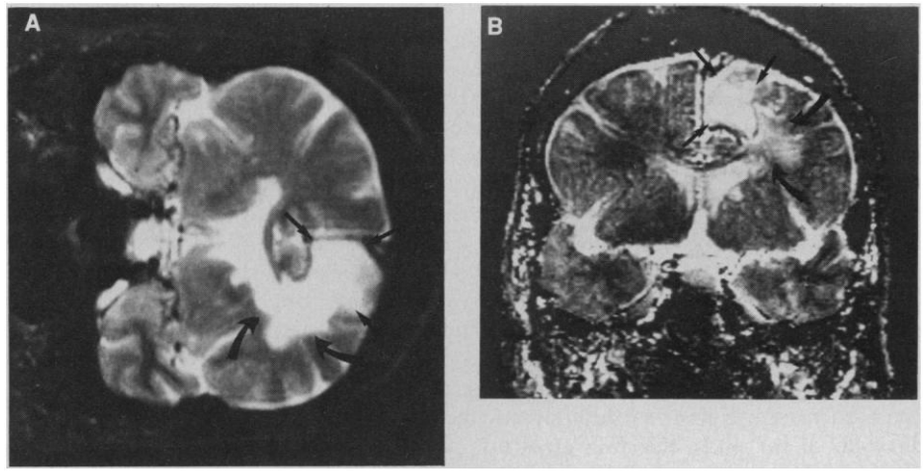

Fig. 4. Coronal images obtained from a patient diagnosed with a benign brain tumor (meningioma). (**A**) Conventional image: the tumor (straight arrows) and surrounding edema (curved arrows) cannot be discriminated. (**B**) Calculated diffusion (IVIM) image. The hyperintense area at the top of the brain corresponds to the tumor. Beneath the tumor, the area of moderately increased intensity corresponds to surrounding vasogenic edema, where water is as mobile as in cerebrospinal fluid in the nearby ventricular cavities. The tumor shows an even greater "apparent diffusion coefficient," tentatively attributed to high perfusion of the tumor. The image was calculated from two spin echo images of 1 mm by 1 mm in plane resolution. Acquisition details: slice thickness, 10 mm; echo time, 140 ms; repetition time, 1700 ms (cardiac gated); diffusion gradients of 35-ms duration and 0.004 T/min in the vertical direction; and field strength, 0.5 T. [Courtesy of D. Le Bihan, Diagnostic Radiology Department, National Institutes of Health, Bethesda, Maryland]

In order to clarify the biophysics of the displacement of water in healthy and diseased tissue, IVIM imaging is often done by a series of images with different gradient strengths. The diffusion coefficient is then determined for each volume element to separate the attenuation due to IVIM from all other resonance characteristics. For example, Fig. 3 was obtained in a cat brain 6 hours after the occlusion of the middle cerebral artery, which is an established experimental stroke model. The affected area is difficult to outline on the conventional image, although some ischemic damage can be seen (Fig. 3A). The stroke region is characterized by a drastically lowered diffusion coefficient of water as compared with healthy brain tissue (Fig. 3B). The physiologic basis for the lowered diffusion coefficient is not entirely understood, but the effect, which has been reported to be visible as early as 45 min (*26*), may be linked to cytotoxic edema. In conventional imaging, abnormalities in ischemic brain tissue are visible only after about 3 hours. Therefore IVIM imaging may be superior to conventional MRI in the early detection of stroke (*26*).

Another example is shown in Fig. 4 for a patient diagnosed with meningioma. On the conventional MRI image, the tumor area and surrounding vasogenic edema at the top of the brain could not be distinguished (Fig. 4A). In the calculated IVIM image (Fig. 4B) the area below the tumor could be identified as vasogenic edema on the basis of the diffusion coefficient resembling that of cerebrospinal fluid. The tumor shows an even higher "pseudo" diffusion coefficient, tentatively attributed to the high perfusion (vide infra) of this tumor (*21*).

Interestingly, the diffusion coefficient in brain is anisotropic, especially in the vicinity of myelin fiber tracts (*26*). Thus the resistance to diffusional motion depends on direction. This effect may be used to characterize tissue. Another application is the noninvasive mapping of temperature (*27*). The basis of this method is the well-established relation between diffusion and temperature. This approach has been suggested to monitor, in real time, hyperthermia treatment of malignant tumors (*24*).

Imaging of Tissue Perfusion

The assessment of capillary circulation or tissue perfusion may be used for evaluating the extent of hypoperfusion in stroke and the degree of malignancy in gliomas. Treatment efficacy can be measured in follow-up examinations of tissue perfusion. Perhaps the most interesting scientific (and in a later stage, clinical) potential is imaging of organ function, especially with respect to adaptation of capillary circulation following a change in stimulus. For example, PET studies have shown that a correlation exists between brain tissue activation and capillary blood flow, which is carrying nutrients like glucose and oxygen (*28*). Similarly, heart function requires adaptation mechanisms for oxygen supply, and therefore sensitive regulation of perfusion of the heart muscle.

Although flow can be measured by MR angiography, attempts to apply this latter technique to perfusion must deal with capillary size, since the diameter of capillaries is orders of magnitude smaller than the diameter of a volume element in MRI. The distribution of capillaries is such that within any volume element the capillary volume fraction is small (of the order of a few percent). Thus any MRI method based only on flowing capillary water must pay a price in sensitivity, and thus in spatial resolution, when compared with conventional MRI. Additional problems in using MR angiographic methods for capillary perfusion are that the flow velocity is rather small and that capillary direction is random to a certain extent, leading to partial cancellation of signal. If the capillary orientation is completely random within one volume element, then the redistribution of capillary blood may be described in a manner similar to the Brownian motion in diffusion and, as proposed recently (*21*), imaged with diffusion (IVIM) imaging techniques.

Because of accuracy problems in detecting effects in only a few percent of the available signal, a higher sensitivity to capillary flow may be obtained with a method in which the stationary water outside the vascular spaces is "influenced" by the capillary flow. The measurement of the passage of a bolus of MRI contrast agent provides such an opportunity (*29*). Contrast agents in MRI are not directly visible but change the magnetic properties of other nuclei in close proximity, such as those of the water hydrogens in MRI. They consist of transition metal or lanthanide series ions with a suitable chelator (*30*). The signal of water can be altered by the contrast agent in two different ways, either by changing the relaxation or through bulk susceptibility effects, or both, as explained below.

The relaxation times (especially T_1, but also T_2) of nearby water hydrogens in the capillaries can be lowered in the presence of contrast agent. The T_1 value in other compartments (intracellular or interstitial) may then be lowered as a result of exchange of water between different compartments or because contrast agent can leak into these compartments. Permeability for contrast agents differs strongly among different organs. In healthy brain, no contrast agent can leak across the blood-brain barrier, whereas in heart, leakage into interstitial spaces can easily occur. Recently, techniques have been proposed that are designed to measure the transient decrease in T_1 of water as an indicator of the passage of contrast agent in

capillaries in heart and brain (*31*).

Bulk magnetic susceptibility (*32*) within an organ can be altered by MRI contrast agents to create differences in magnetic field between the vascular system (where the majority of contrast agent resides during the first passage) and extravascular spaces. These magnetic field differences can be regarded as locally generated magnetic field gradients, which extend beyond the vasculature depending on size, geometry, and distribution of the vessels, and may thus alter the phase of the transverse magnetization of all water nuclei in a volume element. In addition, as nuclei move through the locally generated gradient, their resonance frequencies and phase change in proportion to it (*33*).

The relaxation and susceptibility effects of contrast agents are often hard to separate, thus making it difficult to relate signal intensity to concentration of contrast agent, a necessary element in the quantification of flow. In addition, the information does not reflect exclusively capillary circulation but includes flow in larger vessels as well. Quantification is further complicated because an ideal bolus of contrast agent is difficult to achieve, and the measured time dependence curves reflect the organ transit function superimposed on the arterial input function. However, recent results indicate that information on blood volume and capillary flow may be obtained with such methods (*33*). By tracking the time dependence of neighboring volume elements, flow direction and history may also be detected (*34*). Since the transit times of intravascular contrast agents in brain is of the order of a few seconds, fast imaging techniques, which acquire an image in a period of about 1 to 2 s, are necessary.

Images of monkey brain following a bolus injection of contrast agent [dysprosium diethylene triamine pentaacetic acid–bis methyl amide (DTPA-BMA)] are shown in Fig. 5. Each image was collected in 1.9 s, which permitted the measurement of time curves of regional inflow and outflow. The signal decrease due to the passage of the intravascular contrast agent can be dramatic (≥80% in many volume elements only 14 s after injection) and the normally high spatial resolution of MRI can be maintained in these perfusion-sensitized images.

Another example of the use of dynamic contrast is the identification of abnormal kidney function (*35*). The paramagnetic contrast agent (gadolinium DTPA) acts as a filtration marker that is freely filtered by the kidney. The passage of this agent through the renal vasculature into the tubules and collecting ducts demonstrates a pattern of contrast that is readily explained based on the relevant anatomy, physiology, and function of the parts of the nephron. This result indicates the possibility of MRI as a screening technique for nephrotoxic side effects of new pharmacological agents. A second application is the study of cerebral perfusion. Differences in white and gray matter have been observed as well as changes in perfusion upon alterations in arterial pCO_2 (*33*). Preliminary work in an animal model of unilateral occipital cortical blindness has shown differences in cerebral blood volume in response to visual stimulation between intact and blinded cortices (*36*).

Contrast agents in MRI are also used to evaluate the integrity of the blood-brain barrier. They can leak through a rupture into brain tissues and lower the relaxation times of water hydrogens (especially T_1, but also T_2). Future developments in functional MR contrast agents will likely involve the design of pure intravascular agents (bound to macromolecules) (*37*) that may be used to study heart and tumor perfusion or target specific agents that are dependent upon tissue uptake and excretion. Labeling of antibodies may become feasible. Compounds that can be altered in vivo may also lead to an understanding of organ physiology and pathological processes.

Alternative NMR methods for studying capillary perfusion use magnetically labeled compounds that are directly visible by NMR and whose concentration dependence on time can be interpreted by flow parameters (*38*). Because of the small volume fraction of capillary blood, such methods have a limited spatial resolution. However, they have the advantage that exchange between the

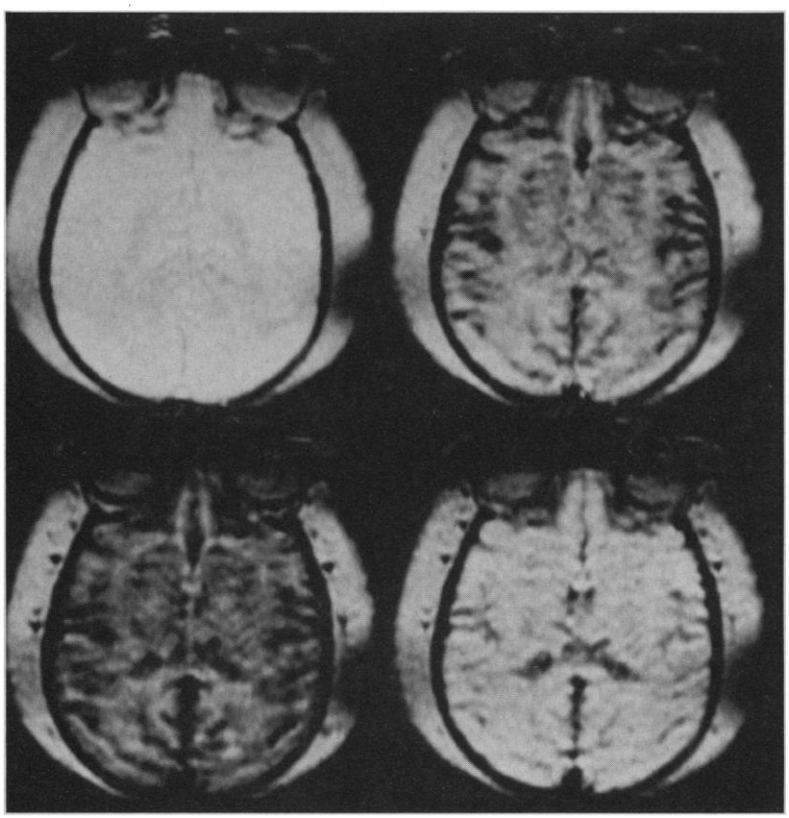

Fig. 5. Imaging of tissue perfusion of the monkey head in transverse direction. At time $t = 0$ (upper left), a bolus of contrast agent (dysprosium DTPA-BMA, 0.8 mmol per kilogram of body weight) was injected in a leg vein. The images at time 10 s (upper right), 14 s (lower left), and 20 s (lower right) show the passage of contrast agent. Acquisition details: gradient recalled echo images; echo time, 11 ms; repetition time, 20 ms; total acquisition time per image, 1.9 s; slice thickness, 5 mm; resolution, 0.6 mm by 0.6 mm in the plane; and field strength, 1.5 T. [Courtesy of J. Frank, D. Doudet, R. Saunders, and T. Aigner, National Institutes of Health, Bethesda, Maryland. Contrast agent was provided by Salutar, Inc., Sunnyvale, California]

capillary spaces and other extra- and intracellular spaces can be taken into account more directly.

Both PET and SPECT are currently used for assessing perfusion. Each makes use of a bolus of radioactive material, which limits the possibility of repeated examinations in a patient. Their spatial and temporal resolution is less than that of MRI, but quantification of perfusion is more straightforward.

Imaging of Exchange

Water exchange processes can be visualized by MRI (*39*). The principal information source is the longitudinal magnetization. The method relies on the nuclei of interest being in at least two pools with different properties. If a resonance frequency can be found that is characteristic for nuclei from one pool, their longitudinal magnetization can be perturbed selectively by simply applying RF irradiation at that particular resonance frequency. The nuclei in the other pools are unperturbed unless there is a mechanism of exchange (*40*). In the latter case, the perturbation is carried over to the other pools, or, in other words, a magnetization transfer between pools is accomplished. Therefore the technique was named magnetization transfer contrast (MTC) imaging (*39*).

The application to imaging of tissue water is possible because it can, in first approximation, be described by two pools, one characterized by water hydrogens in a relatively "free" state and the other in an "immobilized" state, corresponding to water molecules in close association with membranes or macromolecules. Since the resonance linewidth of hydrogens of free water is relatively narrow compared with that of bound water, one can selectively perturb the hydrogens of bound water by applying RF irradiation at a frequency well beyond the resonance of the hydrogens of free water but within that of bound water. Because of exchange of water between the pools, the perturbation is transferred from the almost invisible pool of bound water to the easily observed pool of free water. Apart from chemical reactions, other mechanisms of exchange may be involved (*41*). Recent studies suggest that the mechanism of physical displacement of water between the pools may be an important factor in the size of the observed effects (*42*). Thus the information content may be complementary to diffusion imaging, since it is visible only if a molecule moves from one pool to another. Although the exact mechanism is not entirely clear, the technique may have an important advantage over diffusion imaging: the source of information is the longitudinal magnetization (and not phase), implying that the method is less sensitive to macroscopic motion. However, interpretation in terms of a single functional parameter may prove difficult because of the many possible processes involved. Some initial results for the cat head are shown in Fig. 6, where the image obtained with and without magnetization transfer contrast displays intensity differences. Muscle tissue has the largest decrease in intensity, followed by white and gray matter, whereas CSF is hardly attenuated.

Imaging of Metabolites

In many diseases, the magnetic properties of water hardly change in comparison with healthy tissue. For example, conventional MRI of water has a disappointingly low contrast for hypoxic insults. However, some metabolites may show dramatic differences in concentration upon alteration in physiology or function. For instance, lactate, phosphocreatine, free phosphate, and adenosine triphosphate (ATP) change by an order of magnitude in concentration in early stages of ischemia (*43, 44*). Since these metabolites are easily identified by the particular chemical shift (Eq. 2) of one or more of their nuclei, they can be measured noninvasively with MRI methods by adding a chemical shift dimension, often referred to as spectroscopic or chemical shift imaging methods.

In 1974, metabolites were detected for the first time by NMR spectroscopy in intact muscle (*45*). In the following years, emphasis was on the measurement of the phosphorus nucleus because of the importance of phosphorylated compounds in cellular energetics. A ^{31}P NMR spectrum allows the determination of the relative concentrations of ATP, free phosphate, and phosphocreatine and the in situ

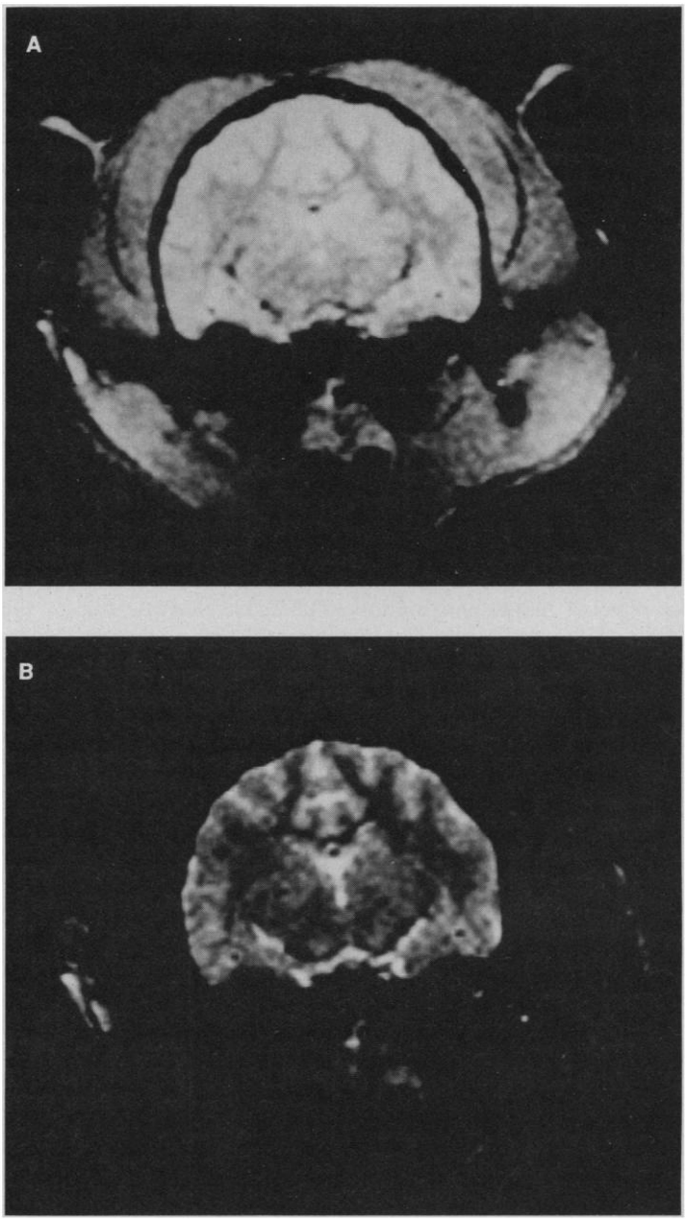

Fig. 6. Exchange weighted coronal images of the cat head. (**A**) Conventional MRI image. (**B**) Magnetization transfer contrast. The difference between the images is due to the exchange of tissue water between "free" and "immobilized" water. Note that the surrounding muscle tissue shows a large signal attenuation, whereas white and gray matter show a lesser but still appreciable signal difference. Acquisition details: gradient recalled echo images; echo time, 10 ms; repetition time, 420 ms; acquisition time per image, 14 min; slice thickness, 1 mm, resolution, 0.4 mm by 0.4 mm; and field strength, 4.7 T. (A) No additional RF irradiation. (B) 400-ms RF irradiation, 10 kHz off-resonance at 3.7 W. [Courtesy of S. D. Wolff and R. S. Balaban, National Heart, Lung and Blood Institute, National Institutes of Health, Bethesda, Maryland]

assessment of pH. Applications include the study of disorders of energy metabolism, muscle and heart physiology (*43*), and cancer (*46*). However, many important biochemical processes do not involve phosphorus. Other nuclei may provide alternative or additional information. For instance, proton NMR may reveal concentrations of neurotransmitters, osmolites, and glycolysis products (*44*). Labeling with the nonradioactive ^{13}C nucleus (*44*) may be used to unravel biochemical pathways in vivo, similar to conventional labeling with the radioactive ^{14}C nucleus used in other techniques.

High spatial resolution in metabolite images is advantageous, because metabolism may vary regionally (*47*). However, the minimum size of a volume element depends on the NMR signal strength, hence on the concentration of the molecule being studied. For comparison, the concentration of water (with two equivalent hydrogen nuclei) is about 40 M in most tissues, whereas that of lactate (three equivalent hydrogen nuclei) may rise to a maximum of 10 to 30 mM during hypoxia. Therefore, if water can be measured in conventional imaging with volume elements of slightly less than 1 μl, a voxel volume of 1 ml would be about the minimum attainable for lactate. A significant price in resolution must be paid for increased contrast and specific metabolic information.

Although the ideas for metabolite imaging were proposed several years ago (*48*), the methods have been refined only recently in such a way that clinical applications have started. Imaging of phosphorus-containing metabolites has been demonstrated for humans (*49*), but with rather limited resolution (volume elements of ≥15 ml). Proton spectroscopy has an intrinsic 16-fold greater sensitivity, but the overwhelming water and fat resonances often overshadow signals of the less abundant metabolites. However, with increasing technical sophistication (*50, 51*), informative brain metabolite images have recently been obtained clinically (*51*). These studies have been mainly limited to measurement of relative metabolite concentra-

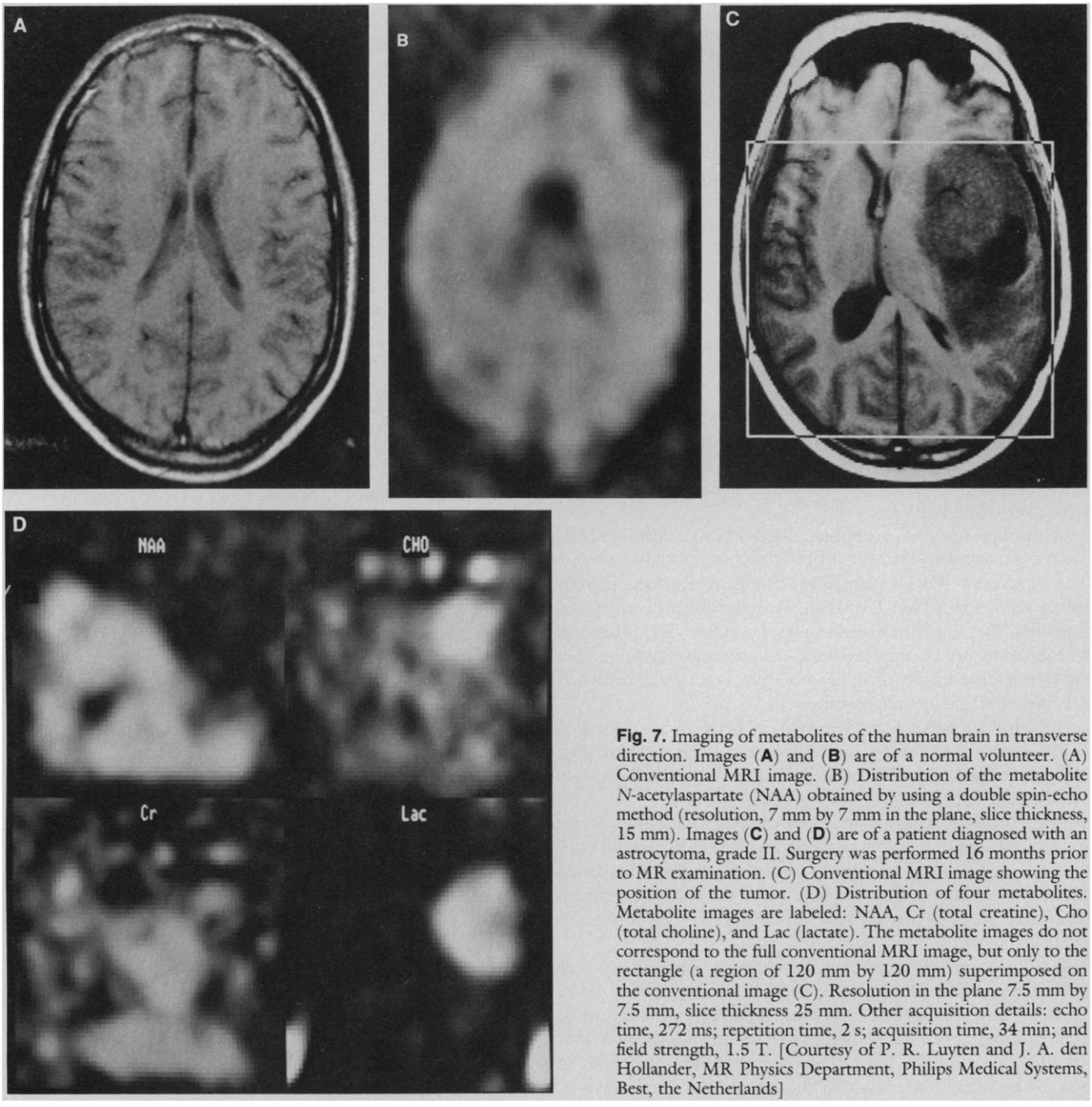

Fig. 7. Imaging of metabolites of the human brain in transverse direction. Images (**A**) and (**B**) are of a normal volunteer. (A) Conventional MRI image. (B) Distribution of the metabolite *N*-acetylaspartate (NAA) obtained by using a double spin-echo method (resolution, 7 mm by 7 mm in the plane, slice thickness, 15 mm). Images (**C**) and (**D**) are of a patient diagnosed with an astrocytoma, grade II. Surgery was performed 16 months prior to MR examination. (C) Conventional MRI image showing the position of the tumor. (D) Distribution of four metabolites. Metabolite images are labeled: NAA, Cr (total creatine), Cho (total choline), and Lac (lactate). The metabolite images do not correspond to the full conventional MRI image, but only to the rectangle (a region of 120 mm by 120 mm) superimposed on the conventional image (C). Resolution in the plane 7.5 mm by 7.5 mm, slice thickness 25 mm. Other acquisition details: echo time, 272 ms; repetition time, 2 s; acquisition time, 34 min; and field strength, 1.5 T. [Courtesy of P. R. Luyten and J. A. den Hollander, MR Physics Department, Philips Medical Systems, Best, the Netherlands]

tions. The value of these methods should increase if information on active metabolism can be incorporated by measuring time evolution of metabolites (*52*).

Some metabolite images in humans are compared with the corresponding conventional images in Fig. 7. *N*-acetylaspartate (NAA) is fairly equally distributed in the brain of a normal volunteer (Fig. 7B), but is dramatically altered in a patient diagnosed with astrocytoma, grade II (Fig. 7D). Large differences are found in the distribution of choline, creatine, NAA, and lactate, possibly indicating regions with rapid cell growth or hypoxia. These regional differences indicate that tumor evaluation with a single volume element may lead to incomplete assessment of metabolism. The same criticism can also be applied to biopsies.

Discussion

Functional imaging has usually been associated with PET, SPECT, ultrasound, computed tomography, and conventional angiography (*53*). Information about flow and perfusion can be obtained from conventional angiography, PET, and SPECT. Metabolic information (for example, glucose turnover) can be obtained by PET. In MRI, a variety of functional parameters can also be incorporated, such as flow, diffusion, capillary perfusion, exchange, and active metabolism. It is therefore useful to address two general questions, namely, the distinctive nature of functional MRI information and its usefulness in clinical medicine or physiology.

The first question has been addressed to some extent in the previous sections, but some general characteristics are summarized here:

1) Except for ultrasound, MRI is the only functional imaging technique that does not use ionizing radiation.

2) MRI images of water have better spatial resolution than images from other methods, except for some conventional angiographic techniques.

3) For imaging of metabolites, the spatial resolution of PET appears slightly superior to MRI of metabolites. However, the different information content of MRI images and potential for encoding active metabolism on different time scales make it a valuable alternative to PET.

4) With respect to small amplitude displacements, diffusion MRI can detect average displacements of the order of micrometers.

5) A functional MRI examination can be performed directly following conventional MRI, enabling straightforward comparison of functional and anatomical parameters. In some cases, functional parameters may even be obtained without appreciable time loss. For example, tissue perfusion imaging with contrast agents takes less than 1 min of actual measuring time.

6) MRI has a relatively low sensitivity. Therefore in contrast to PET, molecules present in low concentration, such as receptor sites, are difficult to locate by MRI, although some advances have been reported recently (*54*).

7) The functional imaging methods discussed here (except for imaging of exchange and time-of-flight angiography) depend critically on the care taken to minimize residual effects from the strong magnetic field gradients that are used. The self-shielded gradient coils (*55*) that are now coming into use can substantially lessen this source of difficulty.

8) Motion during the time that the image is being obtained (a period of the order of a few minutes for conventional MRI techniques) can cause serious problems. Resulting artifacts can be reduced in some instances by using accurate synchronization with the motion (for example, the cardiac or respiratory cycle), but in general the problem of macroscopic motion may be overcome only by methods that significantly reduce the time required to obtain an image. The FLASH method (*8*), with an imaging time of 200 ms to a few seconds, is helpful, and even greater improvements can be expected from current developments in the very fast echo-planar imaging (EPI) technique (*7*), with an imaging time of less than 100 ms.

The question of the usefulness of information provided by functional MRI imaging applies generally to all functional imaging modalities. For research purposes, such information is often crucial to the understanding of function and physiology in healthy and diseased states. The clinical utility of functional MRI in individual patient management can be assessed less readily in this initial phase of its development. However, a few developments are quite promising. For example, in stroke, diffusion MRI appears to detect diseased regions at a much earlier stage than conventional methods. In tumor therapy, imaging of metabolites and of capillary perfusion may provide an earlier indication of the efficacy of the therapy than conventional MRI. It is anticipated that functional MRI will be applied more generally with further advances in very fast imaging, hardware, and specific software.

REFERENCES AND NOTES

1. P. C. Lauterbur, *Nature* **242**, 190 (1973).
2. P. Mansfield and P. G. Morris, *NMR Imaging in Biomedicine* (Academic Press, New York, 1982).
3. P. A. Bottomley *et al.*, *Med. Phys.* **11**, 425 (1984).
4. T. F. Budinger and P. C. Lauterbur, *Science* **226**, 288 (1984).
5. C. B. Higgins, in *Magnetic Resonance Imaging of the Body*, C. B. Higgins and H. Hricak, Eds. (Raven, New York, 1987); M. J. Stehling *et al.*, *Radiology* **170**, 257 (1989).
6. P. van Dyk, *J. Comp. Assisted Tomogr.* **8**, 429 (1984); R. J. Herfliens, C. B. Higgins, H. Hricah, *Radiology* **147**, 749 (1983).
7. P. Mansfield, *J. Phys. C* **10**, L55 (1977).
8. A. Haase *et al.*, *J. Magn. Reson.* **67**, 258 (1986); A. Haase, *Magn. Reson. Med.* **13**, 77 (1990); J. Frahm *et al.*, *ibid.*, p. 150.
9. For general reviews, see R. R. Ernst, G. Bodenhausen, A. Wokaun, *Principles of Nuclear Magnetic Resonance in One and Two Dimensions* (Oxford Univ. Press, Oxford, 1987), pp. 539–564; P. Brunner and R. R. Ernst, *J. Magn. Reson.* **33**, 83 (1979).
10. A. Kumar, D. Welti, R. R. Ernst, *J. Magn. Reson.* **18**, 69 (1975); W. A. Edelstein, J. M. S. Hutchison, G. Johnson, T. W. Redpath, *Phys. Med. Biol.* **25**, 751 (1980).
11. J. R. Singer, *Science* **130**, 1652 (1959).
12. L. Axel, *Am. J. Roentgenol.* **143**, 1157 (1984); W. T. Dixon *et al.*, *Magn. Reson. Med.* **3**, 454 (1986); D. G. Nishimura *et al.*, *ibid.* **4**, 193 (1987).
13. P. R. Moran, *Magn. Reson. Imaging* **1**, 197 (1982); V. J. Wedeen *et al.*, *Science* **230**, 946 (1985); C. L. Dumoulin and H. R. Hart, *Radiology* **161**, 717 (1986); C. L. Dumoulin *et al.*, *Magn. Reson. Med.* **9**, 139 (1989).
14. D. A. Feinberg *et al.*, *Magn. Reson. Med.* **2**, 555 (1985); J. Hennig, M. Düri, P. Brunner, H. Friedburg, *Radiology* **166**, 237 (1988).
15. C. L. Dumoulin *et al.*, *Magn. Reson. Med.* **6**, 275 (1988).
16. G. A. Laub and W. A. Kaiser, *J. Comp. Assisted Tomogr.* **12**, 377 (1988).
17. G. L. Shirman and C. M. Citran, *Am. J. Neuroradiol.* **7**, 3 (1986).
18. G. DiChiro and J. Doppman, *Radiology* **93**, 57 (1969).
19. E. L. Hahn, *Phys. Rev.* **80**, 580 (1950); H. Y. Carr and E. M. Purcell, *ibid.* **94**, 630 (1954).
20. D. Le Bihan *et al.*, *Radiology* **161**, 401 (1986).
21. D. Le Bihan *et al.*, *ibid.* **168**, 497 (1988).
22. J. Andrasko, *J. Magn. Reson.* **21**, 479 (1976); J. E. Tanner, *Arch. Biochem. Biophys.* **224**, 416 (1983); C. T. W. Moonen, P. C. M. van Zijl, D. Le Bihan, D. DesPres, *Magn. Reson. Med.* **13**, 467 (1990).
23. Note that in the original work on diffusion (*19, 24*) as well as most current work, a regular spin echo (following a $90° - \tau_1 - 180° - \tau_1$ pulse sequence) or a stimulated echo (following a $90° - \tau_1 - 90° - \tau_2 - 90° - \tau_1$ pulse sequence) is used, where the diffusion gradients have equal sign and are placed in the τ_1 periods. For the sake of simplicity the effect is here explained for a so-called gradient-recalled echo where the diffusion gradients have opposite sign. The first part dephases and the second part rephases resulting in an "echo," hence its name.
24. E. O. Stejskal and J. E. Tanner, *J. Chem. Phys.* **42**, 288 (1965).
25. D. G. Taylor and M. C. Bushell, *Phys. Med. Biol.* **30**, 345 (1985); K. Merboldt, W. Hänicke, J. Frahm, *J. Magn. Reson.* **64**, 479 (1985).
26. M. E. Moseley *et al.*, *Magn. Reson. Med.* **14**, 330 (1990).
27. D. Le Bihan, J. Delannoy, R. L. Levin, *Radiology* **171**, 853 (1989).
28. M. M. Ter-Pergossian and P. Herscovitch, *Semin. Nucl. Med.* **15**, 377 (1985).
29. A. Villringer *et al.*, *Magn. Reson. Med.* **6**, 164 (1988).
30. R. B. Lauffer, *Chem. Rev.* **87**, 901 (1987).
31. H. L. Kantor *et al.*, paper presented at the Seventh Annual Meeting of the Society of Magnetic Resonance in Medicine, San Francisco, 20 to 26 August 1988; D. J. Atkinson, D. Burstein, R. R. Edelman, *Radiology* **174**, 757 (1990); M. K. Stehling

et al., paper presented at the Eighth Annual Meeting of the Society of Magnetic Resonance in Medicine, Amsterdam, 12 to 18 August 1989.
32. For an introduction on susceptibility effects, see D. G. Gadian, *Nuclear Magnetic Resonance and Its Applications to Living Systems* (Oxford Univ. Press, Oxford, 1982), p. 101; S. C.-K. Chu, Y. Xu, J. A. Balschi, C. S. Springer, Jr., *Magn. Reson. Med.* **13**, 239 (1990); S. Posse and W. P. Aue, *J. Magn. Reson.* **88**, 473 (1990).
33. J. W. Belliveau *et al.*, *Magn. Reson. Med.* **14**, 538 (1990); B. R. Rosen, J. W. Belliveau, D. Chien, *Magn. Reson. Q.* **5**, 263 (1989).
34. G. Sobering *et al.*, paper presented at the Ninth Annual Meeting of the Society of Magnetic Resonance in Medicine, New York, 18 to 24 August 1990.
35. R. Kikinis *et al.*, *Radiology* **165**, 837 (1987); M. J. Carvlin *et al.*, *J. Comput. Assisted Tomogr.* **11**, 448 (1987); P. L. Choyke *et al.*, *Radiology* **170**, 713 (1989).
36. J. A. Frank *et al.*, paper presented at the Ninth Annual Meeting of the Society of Magnetic Resonance in Medicine, New York, 18 to 24 August 1990.
37. M. E. Moseley *et al.*, *J. Comput. Assisted Tomogr.* **13**, 215 (1989).
38. D. Barranco *et al.*, *J. Cerebral Blood Flow Metab.* **9**, 886 (1989); J. R. Ewing *et al.*, *Stroke* **20**, 259 (1989); J. J. H. Ackerman, C. S. Ewy, N. N. Becker, R. A. Shalwitz, *Proc. Natl. Acad. Sci. U.S.A.* **84**, 4099 (1987).
39. S. D. Wolff and R. S. Balaban, *J. Magn. Reson.* **86**, 164 (1990).
40. S. Forsen and R. A. Hoffman, *J. Chem. Phys.* **39**, 2892 (1963).
41. S. D. Wolff and R. S. Balaban, *Magn. Reson. Med.* **10**, 135 (1989).
42. J. A. Helpern *et al.*, paper presented at the Ninth Annual Meeting of the Society of Magnetic Resonance in Medicine, New York, 18 to 24 August 1990.
43. G. K. Radda, *Science* **233**, 640 (1986).
44. J. R. Alger and R. G. Shulman, *Brit. Med. Bull.* **40**, 160 (1984); J. W. Prichard and R. G. Shulman, *Annu. Rev. Neurosci.* **9**, 61 (1986).
45. D. I. Hoult *et al.*, *Nature* **252**, 285 (1974).
46. P. F. Daly and J. S. Cohen, *Cancer Res.* **49**, 770 (1989); J. D. Glickson, *Invest. Radiol.* **24**, 1011 (1989); M. W. Weiner, *ibid.* **23**, 253 (1988).
47. G. DiChiro, *Invest. Radiol.* **22**, 360 (1987).
48. T. R. Brown, B. M. Kincaid, K. Ugurbil, *Proc. Natl. Acad. Sci. U.S.A.* **79**, 3523 (1982); A. A. Maudsley *et al.*, *J. Magn. Reson.* **51**, 147 (1983).
49. T. R. Brown, S. D. Buchthal, J. Murphy-Boesch, S. J. Nelson, J. S. Taylor, *J. Magn. Reson.* **82**, 629 (1989); A. A. Maudsley *et al.*, *Magn. Reson. Med.* **14**, 415 (1990); P. A. Bottomley *et al.*, *ibid.* **7**, 319 (1988); R. E. Lenkinski *et al.*, *Radiology* **169**, 201 (1989); J. S. Troop *et al.*, *ibid.*, p. 207; D. R. Bailes *et al.*, *J. Magn. Reson.* **74**, 158 (1987).
50. C. M. Segebarth, D. F. Baleriaux, P. R. Luyten, J. A. den Hollander, *Magn. Reson. Med.* **13**, 62 (1990); J. Frahm *et al.*, *ibid.* **9**, 79 (1989).
51. P. R. Luyten *et al.*, *Radiology*, in press.
52. B. D. Ross *et al.*, *N. Engl. J. Med.* **304**, 1338 (1981); T. R. Brown, K. Ugurbil, R. G. Shulman, *Proc. Natl. Acad. Sci. U.S.A.* **74**, 5551 (1977); P. S. Hsieh and R. S. Balaban, *J. Magn. Reson.* **74**, 574 (1987). D. L. Rothman *et al.*, paper presented at the Eighth Annual Meeting of the Society of Magnetic Resonance in Medicine, Amsterdam, 12 to 18 August 1989; G. I. Shulman *et al.*, *N. Engl. J. Med.* **322**, 223 (1990).
53. A representative example for ultrasound is S. Kaul, *Am. J. Med. Sci.* **299**, 113 (1990); for CT, see D. Gur, W. F. Good, S. K. Wolfson, Jr., H. Yonas, L. Shabason, *Science* **215**, 1267 (1982); for PET, see M. E. Phelps and J. C. Mazziotta, *ibid.* **228**, 799 (1985); for SPECT, see B. L. Holman and S. S. Tumeh, *J. Am. Med. Assoc.* **263**, 561 (1990); for conventional angiography, see W. K. Freeman, R. J. Gibbons, A. A. Bove, *Int. J. Cardiol.* **22**, 339 (1989).
54. R. Weissleder, P. Reimer, A. S. Lee, J. Wittenberg, T. J. Brady, paper presented at the Ninth Annual Meeting of the Society of Magnetic Resonance in Medicine, New York, 18 to 24 August. Book of abstracts, p. 52 (1990).
55. P. Mansfield and B. Chapman, *J. Phys. E* **19**, 540 (1986); R. Turner and R. M. Bowley, *ibid.*, p. 876; P. B. Roemer, W. A. Edelstein, J. S. Hickey, paper presented at the Fifth Annual Meeting of the Society of Magnetic Resonance in Medicine, Montreal, 12 to 18 August 1986.
56. This article would not have been possible without the help and discussions of colleagues in the In Vivo NMR Research Center. In addition, we thank all of the research groups that have contributed to the figures.

Mass Spectrometry and Its Use in Tandem with Laser Spectroscopy

E. R. GRANT AND R. G. COOKS

Mass spectrometry is undergoing rapid development, especially with the extension of its range into the hundreds of kilodaltons, the emergence of the quadrupole ion trap as a high-performance instrument, and the development of techniques for recording three-dimensional spectra. These advances are summarized in this review; in addition, the power of the combination of lasers and mass spectrometers is given particular emphasis. Their combination has contributed recently to chemical dynamics, to the study of cluster structure and reactivity, and to the elucidation of the properties of highly excited molecules and ions.

MASS SPECTROMETRY (MS) IS BOTH A SELF-CONTAINED discipline and an instrumental method used widely in the sciences. This article attempts to provide a snapshot of current activities of both types. In the first part, which covers recent advances in MS, we (i) discuss advances in ion production from biomolecules by laser desorption and by desolvation methods ("spray techniques"), especially those which yield intact multiply charged molecular ions and thereby extend the mass range of mass spectrometers into the tens and even hundreds of kilodaltons without requiring any changes in the instrument itself; (ii) summarize the state of the art in biomolecule structural analysis; (iii) present the rapid evolution of the simple quadrupole ion trap into a high-performance instrument capable of multiple stages of mass analysis (MS^n experiments), very high mass-to-charge (m/z) range, and exquisite sensitivity; (iv) emphasize the exciting multidimensional experiments made possible by multiple analyzer instruments; and (v) present MS evidence for the existence of elusive neutral molecules, including those important in astrochemistry. We further illustrate the applications of MS in the second part through a single representative topic—its use in physical chemistry research, especially in structural and dynamical studies on small molecules in combination with laser spectroscopy. Included is a discussion of laser multiphoton ionization (MPI) and dissociation and its applications to reaction dynamics, the dynamics of reactive scattering, and the properties of cluster species and other ions as elucidated by laser-based MS techniques.

The authors are in the Chemistry Department, Purdue University, West Lafayette, IN 47907.

Recent Advances in Mass Spectrometry

High molecular weight measurement. Traditionally a major application of MS has been the measurement of molecular weights of organic compounds in the mass range below 1000 daltons. The